NEW INSIGHTS INTO THERMAL TIDES FROM MARS CLIMATE SOUNDER INTRACK AND CROSSTRACK DATA. L. J. Steele[1], A. Kleinböhl[1], D. Kass[1] and R. W. Zurek[1], [1]Jet Propulsion Laboratory, California Institute of Technology, Pasadena, California, USA. (liam.j.steele@jpl.nasa.gov)

Introduction: Thermal tides are global-scale oscillations of atmospheric temperature, pressure and wind, which are sub-harmonics of a solar day. They are forced by the absorption of radiation by aerosols, and by heat transfer from the surface. Due to Mars' thinner atmosphere, thermal tides play a much more significant role than on Earth. They influence surface pressure and wind, affect the transport and phase of suspended aerosols, and propagate into the upper atmosphere where they can impact aerobraking maneuvers. As such, it is important to gain a better understanding of their causes and behaviour.

Previous tide analysis has involved the use of computer simulations and spacecraft data, e.g. [1-6]. Analysis of spacecraft data has mostly focused on using temperatures at two local times: ~2am/2pm for Thermal Emission Spectrometer data and ~3am/3pm for Mars Climate Sounder (MCS) data. However, MCS also performed crosstrack scanning, allowing observations at six different local times each day (Fig. 1). These observations have been used to study tides by applying a least-squares fit to the time series data [7-9]. In this work, we perform Fourier analysis on the intrack and crosstrack data to investigate the diurnal and seasonal behaviour of thermal tides.

Methods: We use data from the MCS instrument [10], which provides vertical profiles of temperature, dust and water ice up to ~80 km. Observations with global coverage have been ongoing since 2006, providing six Mars years (MY) of data, with crosstrack observations beginning in MY30. Fig. 1 shows the local time coverage for L_S = 180–190º, MY30. We create average and difference fields from the daytime and nighttime intrack data, as well as the crosstrack data at local times earlier and later than intrack, and perform Fourier analysis on these fields. The resulting amplitudes and phases allow us to compare the evolution of tides at three periods over a time interval of ~3 hours in the tropics, and ~6 hours at ±60º latitude.

Results: While many features in the atmosphere are repeatable year upon year, our results reveal large-amplitude tides in the tropics between L_S = 160–200º in MY29 that do not appear in the intrack data at the same time in other years. Fig. 2 shows a comparison between MY29 and MY30 intrack data (with MY31-33 being similar to MY30). Zonal wavenumbers n = 1–3 show large amplitudes in the MY29 average and difference fields, unlike in other years, with n = 3 having the largest amplitude of ~6 K. The average temperature field in the tropics (Fig. 2, bottom panels) clearly shows the strong wave feature in MY29, centered at

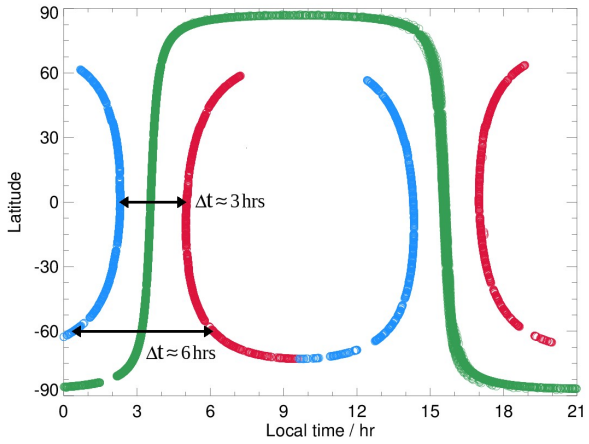

Fig. 1 *Local time coverage of MCS intrack data (green), crosstrack earlier (blue) and crosstrack later (red) observations during the period L_S = 180–190º, MY30.*

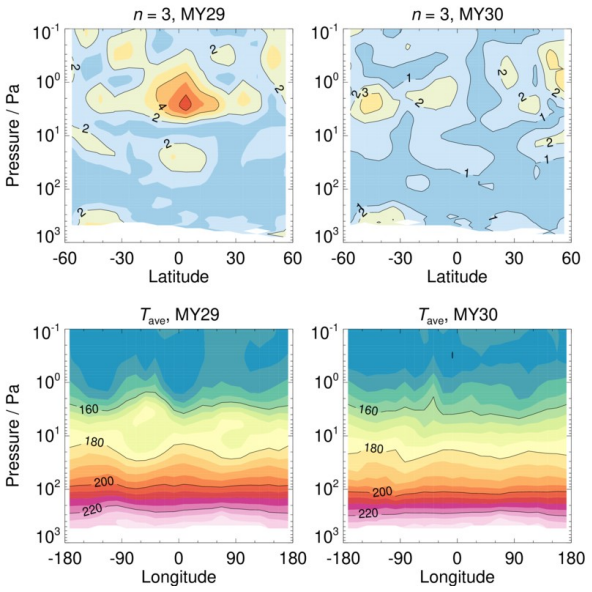

Fig. 2 *(Top panels) amplitude (K) of the zonal wavenumber n = 3 component of T_{ave} = (T_{3am}+T_{3pm})/2 for MY29 and MY30. (Bottom panels) T_{ave} field averaged between ±15º latitude. MCS data cover the period L_S = 180-190º.*

around 3 Pa, which is much less defined in MY30. The Fourier analysis shows a phase increase with height in the large-amplitude region, suggesting a westward tilt.

Fig. 3 shows nighttime MCS temperature, dust and ice distributions from MY29 intrack observations, and MY30 intrack and crosstrack observations. Data are

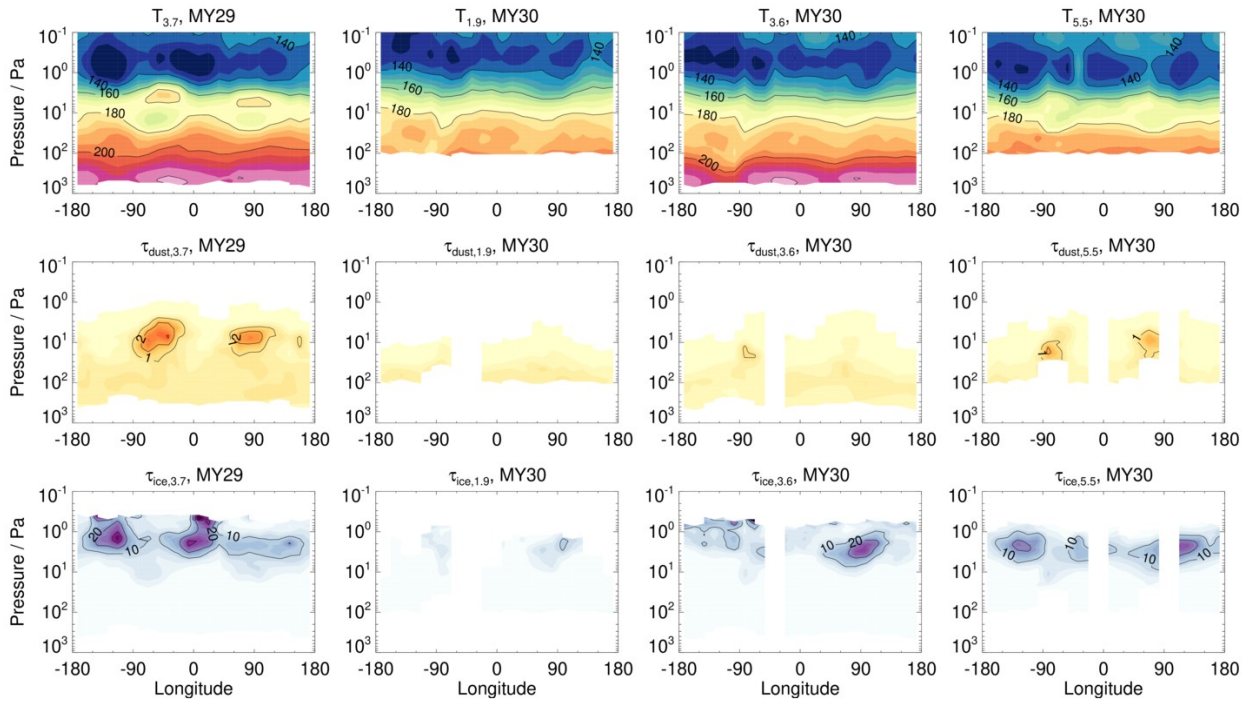

Fig. 3 *Temperature (top row, K), density-scaled dust opacity (middle row) and density-scaled water ice opacity (bottom row) from MCS nighttime data covering the period L_S = 180-190º. Data are averaged between ±15º latitude. MY29 panels show intrack data with an average local time of 3.7am. MY30 panels show intrack data (average time 3.6am) and crosstrack data (average times of 1.9am and 5.5am). Density-scaled opacity has units of 10^{-3} m^2 kg^{-1}.*

averaged over L_S = 180–190º. (The daytime temperature structure in intrack measurements is similar in MY29 and MY30, so not shown.) There is a prominent zonal wavenumber 3 pattern in the MY29 intrack temperature field ($T_{3.7}$), centered at around 3 Pa, which appears to be associated with increased abundances of dust ($\tau_{dust,3.7}$). When compared to the MY30 intrack temperature field ($T_{3.6}$) this wave feature is not apparent, and neither are the increased dust abundances. However, in the crosstrack data, which are for a local time ~2 hours after the intrack data, it can be seen that two regions of increased nighttime dust have appeared in similar locations to those in MY29. The temperature field ($T_{5.5}$) now shows a zonal wavenumber 3 pattern, and Fourier analysis of this field yields similar results to those for MY29 in Fig. 2. The same behaviour is seen in MY30, 31 and 33, with MY32 not having crosstrack data at this time.

To try and understand these results we performed a similar analysis using the Ensemble Mars Atmosphere Reanalysis System (EMARS) data [11]. However, the behaviour seen here is not present in EMARS. This may be due to the use of horizontal dust optical depth maps to constrain the dust cycle, rather than assimilating dust profiles.

Conclusions: MCS crosstrack data reveals features of thermal tides that are not present using intrack data alone, as has been done in most previous studies. Particularly, around southern hemisphere spring equinox there are large-amplitude tidal features in the tropics that appear in MY29 intrack data, but which are present only in crosstrack data in other years. These appear linked to temporal variations in the nighttime dust (and possibly ice) distributions.

Acknowledgements: This work was carried out at the Jet Propulsion Laboratory, California Institute of Technology under a contract with NASA. Copyright 2019, all rights reserved. Government sponsorship acknowledged.

References: [1] Wilson, R. J. and Hamilton, K. (1996) *J. Atmos. Sci.*, 53, 1290-1326. [2] Banfield, D. et al. (2000) *J. Geophys. Res.*, 105, 9521-9537. [3] Lee, C. et al. (2009) *J. Geophys. Res.*, 114, E03005. [4] Moudden, Y. and Forbes, J. M. (2011) *J. Geophys. Res.*, 116, E01004. [5] Guzewich, S. D. et al (2012) *J. Geophys. Res.*, 117, E03010. [6] Guzewich, S. D. et al (2014) *J. Geophys. Res. Planets*, 119, 506-519. [7] Kleinböhl, A. et al. (2013) *Geophys. Res. Lett.*, 40, 1952-1959. [8] Wu, Z. et al. (2017) *J. Geophys. Res. Planets*, 120, 2206-2223. [9] Wu, Z. et al. (2017) *J. Geophys. Res. Planets*, 122, 1227-1242. [10] McCleese, D. J. et al. (2007) *J. Geophys. Res.*, 112, E05S06. [11] Greybush, S. J. et al. (2018) *Geosci. Data J.*, submitted, doi:10.18113/D3W375.